International Geology Review, 2014
Vol. 56, No. 1, 15–28, http://dx.doi.org/10.1080/00206814.2013.818750

Karakoram fault activity defined by temporal constraints on the Ayi Shan detachment, SW Tibet

Shifeng Wang[a]*, Yasi Mo[b,c], Richard J. Phillips[d] and Chao Wang[b,c]

[a]*Institute of Geomechanics, Chinese Academy of Geological Sciences, Beijing 100081, China;* [b]*University of Chinese Academy of Science, Beijing 100049, China;* [c]*Institute of Tibetan Plateau Research, Chinese Academy of Sciences, Beijing 100101, China;* [d]*Institute of Geophysics and Tectonics, School of Earth and Environment, University of Leeds, Leeds LS2 9JT, UK*

(*Accepted 19 June 2013*)

The role of the Karakoram fault (KKF) in evolution of the Tibetan–Himalayan orogenic belt is controversial. Some consider the KKF to be a stable, long-lived feature with several hundred kilometres of offset along its entire current trace, whereas others interpret it as having propagated along its NW–SE trend since initiation at ~16 Ma with small-scale slip being gradually absorbed by transfer structures along the fault trace. Here we report new zircon U–Pb and mica $^{40}Ar/^{39}Ar$ ages related to the Ayi Shan detachment to better constrain the activity of the KKF in southwestern Tibet. The zircon U–Pb data show migmatite ages of 489, 478, and 435 Ma from the footwall of the Ayi Shan detachment involved in the KKF ductile shear zone. Mylonitized migmatite in the South Ayilari did not record any KKF activity. Similarly aged magmatic and metamorphic information recorded in mylonites and undeformed rocks of the Animaqing Group around the North Ayilari also rules out the effect of KKF movement on zircon growth. Cenozoic information recorded in North Ayilari zircons evidently resulted from Trans-Himalayan magmatic belt (THB) magmatism during 45–50 Ma and 32–25 Ma. Four mica dates from the same mylonitized samples all cluster around 12 Ma. Combined zircon U–Pb and mica $^{40}Ar/^{39}Ar$ ages from the mylonites and undeformed rocks support the hypothesis that the KKF imposed a structural fabric on the rocks of the Animaqing Group and the THB granites at around 12 Ma in the Ayilari Range. Chronologic, kinematic, and geometric studies demonstrate that the fault propagated southeastward into SW Tibet at 12 Ma.

Keywords: Karakoram fault; Ayi Shan detachment; Animaqing Group; mylonitized migmatite; U–Pb age; $^{40}Ar/^{39}Ar$ age

Introduction

The NW–SE-trending Karakoram fault (KKF) is one of the most prominent morphologic features in the western Himalayan–Tibetan orogen and central to the debate concerning end member models of continental deformation (Searle *et al.* 2011).

Over the initiation age and evolutionary history of the fault, data that are utilized to critically assess competing models of continental deformation have resulted in contrasting interpretations of faulting and relevance to these competing models. In the extrusion model, the KKF is interpreted as a stable, long-lived feature initiating at 32–25 Ma along its entire current trace, with only minor changes in kinematics (e.g. Peltzer and Tapponnier 1988; Armijo *et al.* 1989; Lacassin *et al.* 2004). In the distributed deformation model, the KKF is interpreted as propagating continuously along its NW–SE trend since initiation (e.g. Searle 1996; Murphy *et al.* 2000; Robinson 2009). Over the last few decades, field and laboratory work has been conducted along different segments of the fault, and great progress has been achieved in investigating its geometric, kinematic, and chronological characteristics (e.g. Armijo *et al.* 1989; Ratschbacher *et al.* 1994; Searle 1996; Searle *et al.* 1998; Phillips *et al.* 2004, 2013; Murphy *et al.* 2000, 2002; Lacassin *et al.* 2004; Robinson *et al.* 2004; Phillips and Searle 2007; Wang *et al.* 2009, 2011, 2012, 2013; Murphy *et al.* 2010; Robinson *et al.* 2012).

Initial characterization of the fault by Peltzer and Tapponnier (1988) and Liu (1993) suggested a fault model that supported the extrusion hypothesis, namely that the fault initiated in the Eocene, had an offset of 1000 km, and a corresponding long-term slip rate of ~30 mm/year. This contrasted strongly with improved fault chronology and mapping by Searle (1996) and Searle *et al.* (1998), who argued that the fault initiation age was significantly later at 18 Ma and displayed a maximum offset of 120–150 km, providing a slip rate of ~8 mm/year. Searle *et al.* (1998) argued that these data did not support the extrusion model because the fault was too young and displayed a limited offset and slip rate. In more recent years, the debate has strengthened as more detailed mapping and chronological techniques have been undertaken along the length of the fault. Laccasin *et al.* (2004) revised the maximum offset to 280–400 km with a slip rate of ~10 mm/year.

Corresponding author. Emails: wsf@cags.ac.cn; wsf@itpcas.ac.cn

Searle and Phillips (2004) argued that the interpretation of Lacassin's offset granites as being 'syn-kinematic' was incorrect, and instead postulated that ∼16 Ma granites were prekinematic, had a maximum offset of 40–120 km and a corresponding slip rate range of 4–10 mm/year. Analysis in the North Ayilari (Zhaxigang), South Ayilari (Namru), and Kunsha areas (Wang *et al.* 2009, 2011, 2012) confirms a late Miocene initiation age of 12 Ma and a low offset of 52 km. Wang *et al.* (2013) further points out that the granites referred in Leloup *et al.* (2013) are part of the Ayi Shan detachment (Sanchez *et al.* 2010; Zhang *et al.* 2011).

The debates on the role of the KKF are more and more dependent on quantitative analysis data on the elements relating to the KKF, and specific data on the blur Ayi Shan detachment and its relationship with the KKF would be valuable. Here we are reporting some new petrologic and chronologic data on the Ayi Shan detachment; next, we discuss its constraints on the activity of the KKF.

Geological setting

The KKF, the Great Counter thrust (GCT) fault and the Ayi Shan detachment are three regional tectonic features in the Ayilari Range (Figure 1). The GCT, also named the South Kailas thrust fault in the Kailas area, is a steady tectonic feature in the study area (Yin *et al.* 1999; Harrison *et al.* 2000; Murphy *et al.* 2010). The fault is a N-directed thrust

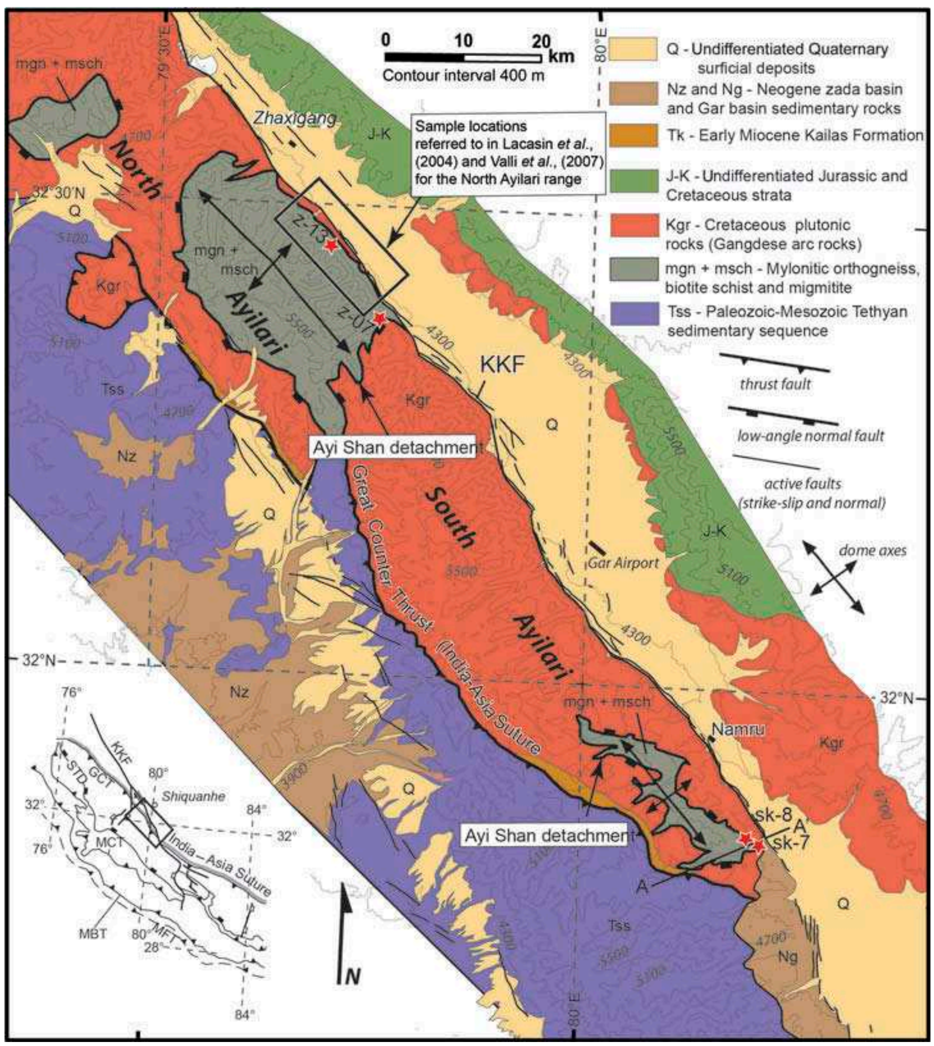

Figure 1. Geologic map of the Ayilari Range showing the first-order geologic structures exposed in the range and location of rock samples analysed by Valli *et al.* (2007, 2008) and Lacassin *et al.* (2004) in the North Ayilari. The red star shows the location of the samples dated in this article.

Notes: GCT, Great Counter thrust; KKF, Karakoram Fault System; MBT, Main Boundary Thrust; MCT, Main Central Thrust; MFT, Main Frontal Thrust; STD, South Tibetan Detachment. Map is compiled from Murphy *et al.* (2000), Xizang BGMR (2005), Sanchez *et al.* (2010), and Wang *et al.* (2011).

fault system, with lenses of serpentinized mafic rocks hundreds of metres long and ultramafic rocks that crop out locally along the fault zone, which defines the surface trace of the Indus-Yalu suture zone. The strata involved in the hanging wall of the GCT are mainly of the Palaeozoic–Mesozoic Tethyan sedimentary sequence, and mélange from the Indus-Yalu suture (Xizang BGMR 2005). The rocks involved in the footwall are mainly different episodes of granites of the Trans-Himalayan magmatic belt (THB; Miller *et al.* 2000; Wang *et al.* 2009, 2011), which form the Ayilari Range topographically. Southeast of Namru village, the Neogene strata of the Namru–Menshi basin overlap the pre-Tertiary rocks, and the sequence of brown and purple sandstones that interbed with grey conglomerate resembles the low magnetostratigraphic sequence in the Zhada basin, which has been dated between 7 and 5 Ma (Wang *et al.* 2008b; Saylor *et al.* 2009). The KKF cuts through the north slope of the Ayilari Range in the Namru–Menshi pull-apart basin, as indicated by the tectonic geomorphology features and ductile shear zones. Between the trace of the GCT and the KKF, the low-angle normal fault of the Ayi Shan detachment is developed (Figure 1), with the THB granite being the hanging wall, mylonitic orthogneiss, biotite schist, and migmatite of the Proterozoic Animaqing Group being the footwall (Xizang BGMR 2005).

Rock samples and analytical methods

Samples were collected from the footwall of the Ayi Shan detachment at the southern and northern extent of the Ayilari Range (Figure 1). The rocks in the Ayi Shan detachment setting show obvious NNW-trending bedding cleavage with moderate dip. The strike of the active KKF parallels the Ayi Shan detachment at the northern slope of the Ayilari Range. The KKF cuts the GCT southeast of Namru village; the relationship between the KKF, the GCT, and the Ayi Shan detachment can be seen in the profile in Figure 2. Samples SK-7, SK-8, and Z-13 represent the mylonitized migmatite melanosome and leucosome (Figure 2), whilst sample Z-07 represents a granodioritic gneiss sampled adjacent to the ductile shear zone.

Zircons were separated by heavy-liquid and magnetic methods at the Laboratory of the Geological Team of Hebei Province, China. Cathodoluminescence (CL) images were then acquired to check the internal structures of individual zircon grains and to select positions for dating analyses. U–Pb dating of zircon from samples SK-7 and SK-8 was conducted using the Chinese Academy of Sciences Cameca IMS-1280 ion microprobe (CASIMS) at the Institute of Geology and Geophysics in Beijing. U–Pb dating of zircon from samples Z-07 and Z-13 was acquired by laser ablation inductively coupled plasma mass spectrometry (LA-ICP-MS) at the Key Laboratory of Continental Collision and Plateau Uplift, Institute of Tibetan Plateau Research, Chinese Academy of Sciences. Both analytical methods follow the procedures of Li *et al.* (2009). The natural zircon reference materials, Plesovice (337 ± 0.37 Ma; Slama *et al.* 2008) and Qinghu (159.45 ± 0.16 Ma, Li *et al.* 2009), were used as external standards for the matrix-matched calibration of U–Pb dating. Weighted mean calculations and probability density plots of U–Pb ages were made using Isoplot/Ex_ver 3 (Ludwig 2001). Table 1 presents the zircon U–Pb dating results.

Four mica samples from SK-7 and SK-8 were selected and purified using a Frantz magnetic separator and conventional heavy organic liquid techniques. Individual grains

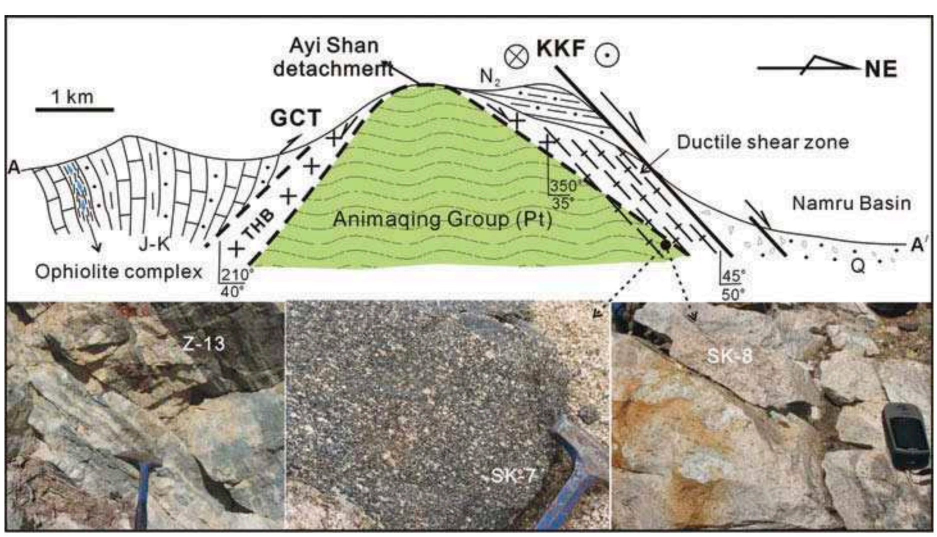

Figure 2. Cross-section through the South Ayilari Range showing the relationship between the Great Counter thrust, Ayi Shan detachment, and the KKF. The Animaqing Group forms the footwall of the GCT and the Ayi Shan detachment and was cut by the movement of the Karakoram fault.

Table 1. CASIMS and LA-ICPMS U–Pb isotopic compositions and ages (Ma) of zircons in samples from the Ayilari Range.

	Concentration (ppm)				U–Th–Pb isotopic ratios						Ages (Ma)					
Spot	Pb*	Th	U	Th/U	$^{207}Pb^*/^{206}Pb^*$	1σ	$^{207}Pb^*/^{235}U$	1σ	$^{206}Pb^*/^{238}U$	1σ	$^{207}Pb^*/^{206}Pb^*$	1σ	$^{207}Pb^*/^{235}U$	1σ	$^{206}Pb^*/^{238}U$	1σ
SK-7																
SK-7@01	99.0	192	522	0.37	0.0737	0.5862	1.6333	1.6166	0.1608	1.5066	1032	12	983	10	961	13
SK-7@02	153.6	71	1864	0.04	0.0563	0.5200	0.5994	1.5904	0.0772	1.5030	466	11	477	6	479	7
SK-7@03	94.8	181	1124	0.16	0.0566	0.6613	0.5945	1.6425	0.0762	1.5034	474	15	474	6	474	7
SK-7@04	51.5	151	598	0.25	0.0571	1.1539	0.5985	1.8925	0.0760	1.5000	496	25	476	7	472	7
SK-7@05	54.6	152	618	0.25	0.0566	1.0083	0.6096	1.8074	0.0781	1.5001	475	22	483	7	485	7
SK-7@06	359.6	165	2017	0.08	0.0714	0.3579	1.6008	1.5440	0.1627	1.5019	968	7	971	10	972	14
SK-7@07	39.2	309	401	0.77	0.0549	1.1538	0.5755	1.8925	0.0761	1.5001	406	26	462	7	473	7
SK-7@08	98.4	414	1064	0.39	0.0571	0.6618	0.6186	1.6395	0.0786	1.5000	496	15	489	6	487	7
SK-7@09	94.2	112	1070	0.11	0.0566	0.6318	0.6302	1.6339	0.0808	1.5068	475	14	496	6	501	7
SK-7@10	138.6	570	641	0.89	0.0746	0.5475	1.6322	1.5992	0.1588	1.5025	1057	11	983	10	950	13
SK-7@11	69.9	193	822	0.23	0.0568	0.8734	0.5895	1.7372	0.0752	1.5017	485	19	471	7	468	7
SK-7@12	142.9	160	1643	0.10	0.0564	0.6279	0.6221	1.6284	0.0800	1.5025	468	14	491	6	496	7
SK-7@13	125.2	78	1615	0.05	0.0565	0.5404	0.5643	1.5951	0.0725	1.5007	471	12	454	6	451	7
SK-7@14	165.4	236	546	0.43	0.0979	0.4398	3.3453	1.5639	0.2478	1.5008	1584	8	1492	12	1427	19
SK-7@15	124.8	190	533	0.36	0.1035	0.4551	2.6917	1.5679	0.1885	1.5004	1689	8	1326	12	1113	15
SK-7@16	87.2	319	355	0.90	0.0768	0.6389	1.9240	1.6320	0.1817	1.5018	1115	13	1089	11	1076	15
SK-7@17	206.4	249	1198	0.21	0.0714	0.4102	1.4941	1.5561	0.1517	1.5011	969	8	928	10	911	13
SK-7@18	74.3	33	999	0.03	0.0568	1.0373	0.5460	1.8250	0.0697	1.5016	484	23	442	7	434	6
SK-7@19	150.3	93	1290	0.07	0.0689	0.6133	1.0122	1.6398	0.1065	1.5208	897	13	710	8	652	9
SK-8																
SK-8@01	22.3	185	218	0.85	0.0570	1.5605	0.6170	2.1646	0.0785	1.5001	491	34	488	8	487	7
SK-8@02	9.2	81	91	0.90	0.0588	2.4078	0.6194	2.8418	0.0764	1.5094	559	52	489	11	475	7
SK-8@03	42.2	130	357	0.36	0.0712	1.0275	0.9549	1.8182	0.0972	1.5000	964	21	681	9	598	9
SK-8@04	133.1	767	1379	0.56	0.0561	0.6177	0.6159	1.6234	0.0796	1.5013	457	14	487	6	494	7
SK-8@05	12.5	95	127	0.74	0.0578	2.6169	0.6141	3.0179	0.0771	1.5032	522	56	486	12	479	7
SK-8@06	80.8	552	760	0.73	0.0574	0.9758	0.6568	1.8287	0.0830	1.5467	507	21	513	7	514	8
SK-8@07	26.3	175	268	0.65	0.0544	1.6609	0.5900	2.2388	0.0787	1.5012	387	37	471	8	488	7
SK-8@08	131.8	314	614	0.51	0.0752	0.5692	1.8267	1.6044	0.1761	1.5001	1074	11	1055	11	1046	14
SK-8@09	23.1	96	240	0.40	0.0610	1.6219	0.6930	2.2109	0.0825	1.5025	638	35	535	9	511	7
SK-8@10	143.0	71	256	0.28	0.1592	0.4316	9.9429	1.5620	0.4531	1.5012	2447	7	2429	15	2409	30
SK-8@11	41.8	269	423	0.64	0.0572	1.2790	0.6237	1.9761	0.0791	1.5064	499	28	492	8	491	7

(*Continued*)

Table 1. (Continued).

	Concentration (ppm)				U–Th–Pb isotopic ratios						Ages (Ma)					
Spot	Pb*	Th	U	Th/U	$^{207}Pb^*/^{206}Pb^*$	1σ	$^{207}Pb^*/^{235}U$	1σ	$^{206}Pb^*/^{238}U$	1σ	$^{207}Pb^*/^{206}Pb^*$	1σ	$^{207}Pb^*/^{235}U$	1σ	$^{206}Pb^*/^{238}U$	1σ
SK-8@12	22.3	180	223	0.80	0.0570	1.5659	0.6072	2.1686	0.0772	1.5003	492	34	482	8	480	7
SK-8@13	45.1	281	461	0.61	0.0568	1.3357	0.6210	2.0091	0.0793	1.5007	484	29	491	8	492	7
SK-8@14	61.2	342	628	0.54	0.0563	0.9596	0.6233	1.7822	0.0803	1.5018	464	21	492	7	498	7
SK-8@15	17.1	93	186	0.50	0.0564	2.1547	0.5973	2.6255	0.0768	1.5001	467	47	475	10	477	7
SK-8@16	213.6	998	2227	0.45	0.0572	0.4836	0.6376	1.5784	0.0808	1.5025	501	11	501	6	501	7
SK-8@17	90.7	486	943	0.52	0.0560	0.8992	0.6161	1.7491	0.0798	1.5002	452	20	487	7	495	7
SK-8@18	201.9	1076	2086	0.52	0.0569	0.5053	0.6319	1.5881	0.0805	1.5056	488	11	497	6	499	7
SK-8@19	78.5	459	798	0.58	0.0565	0.8177	0.6230	1.7085	0.0799	1.5000	473	18	492	7	496	7
SK-8@20	48.4	276	503	0.55	0.0567	1.0984	0.6170	1.8592	0.0790	1.5000	479	24	488	7	490	7
Z07																
Z07-01	5.3	1623	1345	1.21	0.0474	0.0036	0.0232	0.0017	0.0035	0.0001	71	132	23	2	22.8	0.4
Z07-02	48.6	105	528	0.20	0.0648	0.0019	0.7670	0.0211	0.0859	0.0007	768	62	578	12	531	4
Z07-03	17.9	72	135	0.53	0.0681	0.0075	1.1606	0.1268	0.1237	0.0034	871	183	782	60	752	20
Z07-05	70.5	453	567	0.80	0.0638	0.0019	1.0561	0.0294	0.1202	0.0013	734	41	732	15	732	7
Z07-06	48.2	185	400	0.46	0.0686	0.0018	1.1733	0.0287	0.1241	0.0013	886	34	788	13	754	7
Z07-08	76.0	540	922	0.59	0.0577	0.0009	0.6281	0.0091	0.0790	0.0006	519	19	495	6	490	4
Z07-09	67.3	380	1449	0.26	0.0530	0.0009	0.3706	0.0057	0.0508	0.0004	327	21	320	4	319	2
Z07-10	24.1	537	3716	0.14	0.0470	0.0037	0.0456	0.0035	0.0070	0.0001	48	138	45	3	45.2	0.7
Z07-11	95.1	223	852	0.26	0.0667	0.0009	1.1042	0.0121	0.1200	0.0009	830	11	755	6	731	5
Z07-12	183.8	1451	1341	1.08	0.0700	0.0014	1.1931	0.0212	0.1237	0.0011	928	22	797	10	752	6
Z07-13	177.4	312	1273	0.24	0.0697	0.0009	1.4520	0.0159	0.1511	0.0011	920	11	911	7	907	6
Z07-14	108.3	381	1549	0.25	0.0565	0.0007	0.5902	0.0062	0.0758	0.0006	472	11	471	4	471	3
Z07-15	15.6	133	1589	0.08	0.0474	0.0019	0.0652	0.0025	0.0100	0.0001	70	70	64	2	64	0.6
Z07-16	100.5	531	799	0.66	0.0637	0.0009	1.0885	0.0126	0.1241	0.0009	730	12	748	6	754	5
Z07-18	33.4	238	198	1.20	0.0683	0.0024	1.3546	0.0463	0.1439	0.0015	878	53	870	20	867	9
Z07-19	28.7	111	240	0.46	0.0647	0.0020	1.0845	0.0314	0.1216	0.0014	765	42	746	15	740	8
Z07-20	38.4	203	300	0.68	0.0662	0.0030	1.1076	0.0493	0.1215	0.0018	811	69	757	24	739	10
Z07-21	138.2	604	1100	0.55	0.0643	0.0012	1.1035	0.0188	0.1245	0.0011	752	22	755	9	756	6
Z07-22	50.3	23	781	0.03	0.0542	0.0009	0.5543	0.0086	0.0742	0.0006	380	21	448	6	461	4
Z07-23	108.1	335	914	0.37	0.0646	0.0021	1.1062	0.0344	0.1242	0.0011	762	50	756	17	755	6
Z07-24	68.4	188	581	0.32	0.0635	0.0017	1.0673	0.0272	0.1220	0.0013	725	36	737	13	742	7
Z07-25	67.1	231	469	0.49	0.0673	0.0010	1.3080	0.0170	0.1410	0.0011	848	14	849	7	850	6

(*Continued*)

Table 1. (Continued).

Spot	Concentration (ppm)			Th/U	U–Th–Pb isotopic ratios						Ages (Ma)					
	Pb*	Th	U		$^{207}Pb^*/^{206}Pb^*$	1σ	$^{207}Pb^*/^{235}U$	1σ	$^{206}Pb^*/^{238}U$	1σ	$^{207}Pb^*/^{206}Pb^*$	1σ	$^{207}Pb^*/^{235}U$	1σ	$^{206}Pb^*/^{238}U$	1σ
Z13																
Z13-01	16.7	3654	3768	0.97	0.0476	0.0021	0.0309	0.0013	0.0047	0.0001	77	75	31	1	30.4	0.3
Z13-02	73.1	609	630	0.97	0.0640	0.0012	1.0651	0.0174	0.1207	0.0010	742	21	736	9	735	6
Z13-03	30.8	274	1198	0.23	0.0507	0.0023	0.2228	0.0096	0.0319	0.0004	227	77	204	8	202	2
Z13-04	79.3	397	1368	0.29	0.0533	0.0013	0.5191	0.0116	0.0706	0.0006	343	35	425	8	440	4
Z13-05	30.1	33	563	0.06	0.0556	0.0014	0.5292	0.0125	0.0691	0.0006	435	37	431	8	431	4
Z13-06	74.8	244	437	0.56	0.0784	0.0022	2.0548	0.0563	0.1902	0.0019	1157	39	1134	19	1122	10
Z13-07	19.4	55	549	0.10	0.0522	0.0012	0.3260	0.0072	0.0453	0.0004	295	35	287	5	286	2
Z13-08	71.3	199	375	0.53	0.0819	0.0011	2.3839	0.0266	0.2113	0.0016	1242	11	1238	8	1236	8
Z13-09	212.9	366	3901	0.09	0.0532	0.0009	0.5091	0.0072	0.0695	0.0005	336	19	418	5	433	3
Z13-10	57.6	52	1062	0.05	0.0557	0.0009	0.5331	0.0078	0.0694	0.0005	442	20	434	5	432	3
Z13-11	4.7	166	1940	0.09	0.0466	0.0055	0.0194	0.0023	0.0030	0.0001	27	204	20	2	19.5	0.5
Z13-13	27.4	33	493	0.07	0.0583	0.0018	0.5581	0.0168	0.0695	0.0007	540	48	450	11	433	4
Z13-14	53.4	119	613	0.19	0.0614	0.0009	0.8820	0.0118	0.1042	0.0008	653	16	642	6	639	4
Z13-15	84.9	146	689	0.21	0.0684	0.0017	1.3711	0.0326	0.1453	0.0014	882	33	877	14	875	8
Z13-17	166.6	393	1545	0.25	0.0647	0.0007	1.1187	0.0100	0.1255	0.0009	763	9	762	5	762	5
Z13-18	29.6	150	1494	0.10	0.0493	0.0024	0.1587	0.0075	0.0234	0.0002	161	90	150	7	149	2
Z13-19	108.6	259	1788	0.14	0.0618	0.0016	0.5961	0.0146	0.0700	0.0007	665	36	475	9	436	4
Z13-20	20.8	38	829	0.05	0.0505	0.0028	0.2156	0.0117	0.0310	0.0004	216	102	198	10	197	3
Z13-21	16.0	72	2618	0.03	0.0470	0.0031	0.0481	0.0031	0.0074	0.0001	51	121	48	3	47.7	0.5
Z13-22	70.6	242	545	0.44	0.0674	0.0011	1.3008	0.0181	0.1400	0.0011	850	17	846	8	845	6
Z13-23	35.7	93	583	0.16	0.0563	0.0032	0.5562	0.0304	0.0717	0.0011	463	93	449	20	446	7
Z13-24	182.6	87	3171	0.03	0.0554	0.0007	0.5367	0.0052	0.0702	0.0005	430	11	436	3	438	3
Z13-26	128.7	147	2175	0.07	0.0544	0.0007	0.5282	0.0058	0.0704	0.0005	389	13	431	4	439	3
Z13-27	67.1	187	1974	0.09	0.0512	0.0010	0.2891	0.0052	0.0410	0.0003	251	28	258	4	259	2
Z13-28	61.3	341	442	0.77	0.0667	0.0011	1.2728	0.0192	0.1384	0.0011	829	19	834	9	836	6
Z13-29	25.2	121	385	0.31	0.0570	0.0033	0.5469	0.0311	0.0697	0.0011	490	97	443	20	434	7
Z13-30	73.0	97	1243	0.08	0.0555	0.0024	0.5224	0.0216	0.0683	0.0009	432	69	427	14	426	5

Note: Isotopic ratios and ages were corrected by common lead, following the methods reported by Andersen (2002).

were then selected under a binocular microscope. Using an atomic reactor belonging to the Research Institute of Atomic Energy of China, we set the mica samples, a Fish Canyon Tuff sanidine (standard), and a ZBH biotite (132.9 ± 1.3 Ma, standard sample in China) in an H8 hole for fast neutron irradiation. Irradiation lasted 36 h with a total neutron dose of 2.65 E13 n for targeted minerals. We co-irradiated pure salts of K_2SO_4 and CaF_2 with values of ($^{40}Ar/^{39}Ar$) $K = 0.002004$, ($^{39}Ar/^{37}Ar$) $Ca = 0.00081$, and ($^{37}Ar/^{36}Ar$) $Ca = 0.0002398$ to calculate any interfering nuclear reactions of K and Ca. Samples were loaded in aluminium packets and placed into a double vacuum furnace and step heated in the classic fashion, usually from 750°C to 1350°C. The gas was purified by means of Ti and Al–Zr getters. Once cleaned, the gas was introduced into a Helix mass spectrometer at the Institute of Tibetan Plateau Research, CAS. Four to five minutes were allowed for equilibration before performing static analyses. Measured mass spectrometric ratios for $^{40}Ar/^{39}Ar$ analysis were extrapolated to zero time, normalized to the $^{40}Ar/^{36}Ar$ atmospheric ratio, and corrected for neutron-induced ^{40}Ar from potassium and ^{39}Ar and ^{36}Ar from calcium. We calculated dates and errors using formulae recommended by Steiger and Jager (1977). The computer program used for calculations comes from the Berkley Geochronological Center (Ludwig 2001). Table 2 presents the mica $^{40}Ar/^{39}Ar$ dating results.

Results of zircon U–Pb and mica $^{40}Ar/^{39}Ar$ dating

Zircon U–Pb age

Zircons from sample SK-7 appear light pink or colourless and prismatic (~100–300 μm long), and show clear oscillatory zoning and inherited cores (Figure 3). Of the 19 zircon grains dated in this sample, 11 grains with clear oscillatory zoning have Th/U ratios varying from 0.08 to 0.89 and yield concordant $^{206}Pb/^{238}U$ ages of 434–501 Ma (Table 1), with a mean of 478 ± 6 Ma [mean square of weighted deviation (MSWD) = 0.86] (Figures 4A and 4B). We interpret this to be the crystallization age. Six of the remaining eight analyses on the inherited cores plot along the concordian diagram line and yield ages ranging from 652 Ma to 1427 Ma (Figure 4B). These inherited zircon cores are interpreted as reflecting stages in the tectonomagmatic history of the terrane.

Zircons from sample SK-8 are light pink or colourless and prismatic (~100–300 μm long), and show clear oscillatory zoning and inherited cores (Figure 3). Of the 20 zircon grains dated in this sample, 17 grains with clear oscillatory zoning have Th/U ratios varying from 0.28 to 0.9 and yield concordant $^{206}Pb/^{238}U$ ages between 475 and 514 Ma (Table 1), with a mean of 489 ± 5 Ma (MSWD = 1.5) (Figure 4C). We interpret these ages to represent granite crystallization. Results from two of the remaining three analyses of inherited cores plot along the concordia line and yield inherited core ages of 1046 Ma and 2409 Ma (Figure 4D), reflecting the earlier tectonomagmatic history of the terrane.

Zircons in sample Z-07 are light pink or colourless and prismatic, with clear oscillatory zone and inherited cores (Figure 3). Thirteen of the 22 reliable grain data, whether in rims or in cores, yield mean concordant $^{206}Pb/^{238}U$ ages of 746.1 ± 6.9 Ma (MSWD = 2.4), with their Th/U ratios varying from 0.15 to 1.2 (Table 1, Figures 4E and 4F). We interpret these ages to represent the crystallization period of granodioritic gneiss forming during the late Proterozoic. Three data samples from zircon cores are from 850 Ma to 907 Ma, indicating an inherited core from an older tectonomagmatic source. Four data samples from oscillatory rims are around 470 Ma with their Th/U ratios between 0.2 and 0.5, indicating a magmatic activity. Additionally, two individual data samples from the oscillatory rims are 45 Ma and 22.8 Ma, with Th/U ratios of 0.14 and 1.2, showing later magmatism during the Cenozoic.

Zircons in sample Z-13 are light pink or colourless and prismatic, most with clear oscillatory zone and inherited cores (Figure 3). Eleven of the 27 reliable grain data, whether in rims or in cores, yield mean concordant $^{206}Pb/^{238}U$ ages of 435.1 ± 2.9 Ma (MSWD = 1.3), with their Th/U ratios varying from 0.03 to 0.29 (Table 1, Figures 4G and 4H). Eight data samples from zircon cores are from 639 Ma to 1236 Ma, indicating an inherited core from an old tectonomagmatic source. Four data samples from the oscillatory rims are 149 Ma to 286 Ma, indicating that they experienced later magmatic events. Younger rims are dated at 47.7 Ma, 30.4 Ma, and 22.8 Ma, with Th/U ratios of 0.05 to 0.97 showing magmatic or metamorphic fluid activity.

Mica $^{40}Ar/^{39}Ar$ results

Four mica samples from the mylonitic migmatites were collected for $^{40}Ar/^{39}Ar$ measurements (see Figure 1 for sample sites). The mica samples display a plateau defined for about 90% of the ^{39}Ar released at 11.8 ± 0.2 Ma, 12.3 ± 0.2 Ma, 12.4 ± 0.2 Ma, 12.1 ± 0.2, and 11.6 ± 0.1 Ma, respectively (Table 2, Figure 5). Isochron and plateau ages of these samples agree within error. We conclude that the plateau ages in Figure 5 provide meaningful cooling ages and that they reflect distinct episodes of the Ayilari granitoid emplacement.

Discussion

Chronological data on Ayi Shan detachment

The SK-7 and SK-8 samples have similar ages analysed from zircon rims and cores, indicating that the migmatites were formed around 490 Ma. Some of the zircons have

Table 2. $^{40}Ar/^{39}Ar$ stepwise-heating results for mica.

Temp °C	40(r)/39(k)	$^{40}Ar/^{39}Ar$	$^{37}Ar/^{39}Ar$	$^{36}Ar/^{39}Ar$	$^{40}Ar(r)$ (%)	$^{39}Ar(k)$ (%)	Age (Ma)	± 2s
SK-7 Biotite ($J = 0.0004520$)								
750°C	13.180689	55.43576	5.75978	0.14458	23.67	4.68	10.7	1.5
830°C	14.156731	20.25756	1.62977	0.0211	69.79	30.78	11.5	0.3
880°C	14.223743	16.01217	0.11572	0.00608	88.82	16.24	11.6	0.2
930°C	14.441703	15.57706	0.01064	0.00384	92.71	8.24	11.8	0.2
980°C	14.231744	15.77026	0.31554	0.00529	90.22	8.41	11.6	0.2
1030°C	14.287921	17.1668	1.19964	0.01007	83.15	10.96	11.6	0.2
1070°C	14.36712	18.74942	2.01966	0.01539	76.5	14.48	11.7	0.2
1100°C	14.069127	18.25116	0.21793	0.01421	77.07	4.56	11.5	0.3
1200°C	14.365274	18.59523	0.31469	0.0144	77.23	1.49	11.7	0.6
1450°C	8.686818	48.37142	49.2078	0.20374	17.24	0.16	7.1	8.3
SK-7 Muscovite ($J = 0.0004626$)								
750°C	14.474355	35.40243	0.58829	0.07099	40.87	0.99	12.1	1.0
830°C	14.070704	24.28116	2.2292	0.03517	57.84	2.76	11.7	0.5
880°C	13.68839	44.92706	6.02987	0.10738	30.32	5.5	11.4	1.1
930°C	14.645723	26.94918	0.7502	0.04184	54.31	21.32	12.2	0.4
970°C	14.612688	17.97469	0.29944	0.01146	81.28	21.53	12.2	0.2
1010°C	14.295238	19.8445	2.08942	0.01936	71.91	16.22	11.9	0.3
1060°C	14.322671	22.70977	4.82686	0.02973	62.82	10.81	11.9	0.4
1130°C	14.636662	20.89005	3.88208	0.02225	69.84	12.89	12.2	0.3
1250°C	14.445119	17.12414	2.67208	0.00981	84.17	6.42	12.0	0.2
1450°C	11.96461	19.53218	9.93494	0.02832	60.76	1.57	10.0	0.9
SK-8 Biotite ($J = 0.0004335$)								
750°C	15.475673	44.43541	5.36001	0.09951	34.68	6.14	12.1	1.0
830°C	15.561513	20.50716	1.18499	0.01707	75.81	31.23	12.2	0.2
880°C	15.791823	17.17114	0.57541	0.00483	91.92	11.39	12.3	0.2
930°C	16.106989	17.15252	0.36894	0.00364	93.88	7.35	12.6	0.2
980°C	16.004798	17.69079	0.26649	0.00578	90.45	8.14	12.5	0.2
1020°C	15.900965	17.54051	0.61837	0.00572	90.61	12.96	12.4	0.2
1060°C	15.88645	18.6305	0.17522	0.00933	85.26	11.89	12.4	0.2
1100°C	16.224857	19.16052	0.00777	0.00993	84.68	7.52	12.7	0.2
1170°C	17.149416	19.01235	2.1791	0.00692	90.04	2.96	13.4	0.3
1450°C	5.840577	37.24366	92.9616	0.13007	14.5	0.42	4.6	5.3
SK-8 Muscovite ($J = 0.0004417$)								
750°C	21.934298	31.43554	26.90717	0.04022	68.25	1.18	17.4	0.8
830°C	17.08225	22.5743	5.88598	0.02027	75.31	3.56	13.6	0.3
880°C	15.674134	28.84741	3.38458	0.04553	54.19	5.53	12.5	0.5
930°C	15.254797	26.69203	0.87045	0.03895	57.11	24.02	12.1	0.4
980°C	15.269595	18.29049	0.92414	0.01048	83.42	26.09	12.2	0.2
1020°C	15.168045	20.13507	1.895	0.01734	75.22	14.75	12.1	0.3
1060°C	15.556861	22.89403	1.88956	0.02536	67.85	6.44	12.4	0.4
1120°C	15.774095	22.32232	2.67801	0.02291	70.51	7.17	12.6	0.3
1200°C	15.660113	17.94322	0.66286	0.00791	87.23	9.45	12.5	0.2
1300°C	17.27145	18.86267	1.45148	0.0058	91.46	1.81	13.7	0.7

Note: r, radiogenic ^{40}Ar; k, potassium feldspar.

inherited Proterozic cores, reflecting an older tectono-magmatic history. The micas from samples SK-7 and SK-8 are obviously authigenic minerals that recorded the latest tectonic event that the rock experienced. The samples Z-13 have similar ages to SK-7 and SK-8, and inherited Proterozoic cores. Moreover, the zircons in the Z-13 sample had a growth margin of different generations, indicating that the granodioritic gneiss had undergone metamorphism and magmatism around 149–268 Ma, 47 Ma, and 20 Ma, respectively. Z-07 yielded mean ages of 746.1 ± 6.9 Ma, and is concordant with the age attributed to the Animaqing Group (Xizang BGMR 2005). The Z-07 rim records a 490 Ma magmatic event, as seen in samples of SK-7, SK-8, and Z-13. The zircon also records magmatism at 45 Ma and 22 Ma, as in Z-13.

Because the Ayi Shan detachment is characterized by the THB granites as the hanging wall and the Animaqing Group as the footwall, it seems its activity time should be sometime later than the 32–25 Ma period, which is the latest intrusion time of the THB around the Ayilari Range (Wang *et al.* 2011). Valli *et al.* (2007) obtained a 14 Ma mica $^{40}Ar/^{39}Ar$ age from the North Ayilari section, which

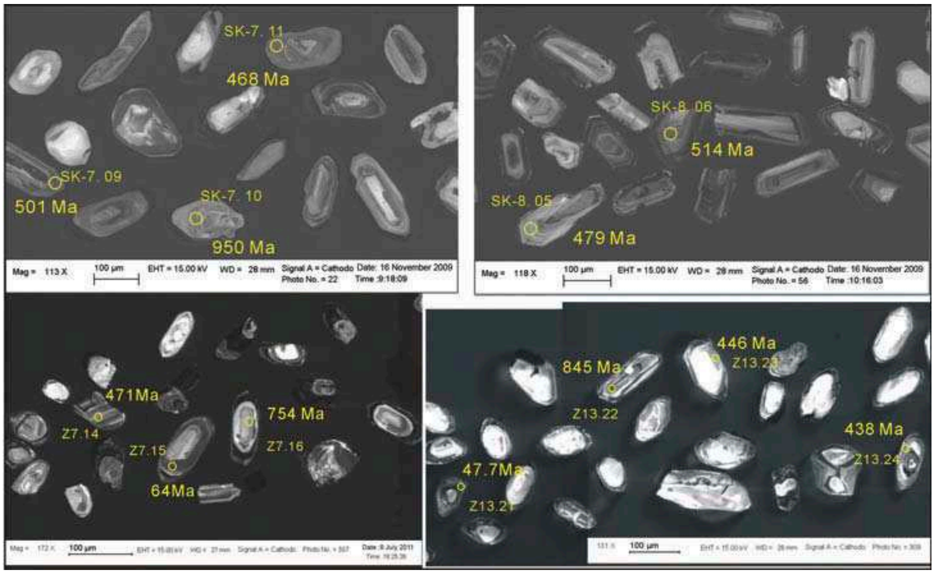

Figure 3. Cathodoluminescence images of sample zircons, with age dates reported in the text.

we attribute to the initiation time of the Ayi Shan detachment (Wang *et al.* 2013). The initiation time of the Ayi Shan detachment is similar to the initiation of the gneiss domes in southern Tibet such as the Kangmar and Kampa Domes (e.g. Chen *et al*. 1990; Lee *et al.* 2000; Queigley *et al*. 2006), implying similar tectonic backgrounds in the Himalayan Orogen in the Miocene.

Since the Proterozoic and Ordovician migmatitite and granodioritic gneiss lies north of the Yarlung-Zangpo suture, they should be part of the Lhasa block basement rocks. The Lhasa block basement is well known for its Permo-Carboniferous metasedimentary rocks (Xizang BGMR 1993). Until now, only one location of Ordovician magmatism has been reported within the north edge of the Lhasa block (Ji *et al.* 2009; Zhu *et al.* 2012). These papers report zircon U–Pb ages of ~493 Ma, similar to the zircon U–Pb ages shown in this study. The discovery of the Proterozoic and Ordovcian migmatitite and granodioritic gneiss around Ayilari Range will benefit the study of the evolutionary history of the Lhasa block.

Chronological constraint on activity of KKF

The new Zircon U–Pb ages reported in this study confirm that the Proterozoic to Ordovician rocks in the footwall of the Ayi Shan detachment are part of the Ayilari Ranges (Xizang BGMR 2005; Sanchez *et al.* 2010; Zhang *et al.* 2011; Wang *et al.* 2013). Previous research has shown that the Ayilari Range consisted mainly of three episodes of granites at ~60 Ma, 45–50 Ma, and 32–25 Ma (Lacassin *et al.* 2004; Valli *et al.* 2007, 2008; Wang *et al.* 2009, 2011). Additionally, the mylonites at the North Ayilari are mainly granitic with a 32–25 Ma zircon U–Pb age. Whilst some authors attribute the 32–25 Ma granite to be part of the THB (Wang *et al.* 2011), others suggest that this reflects syn-kinematic granitoid magmatism associated with initiation of the KKF (Lacassin *et al.* 2004; Valli *et al.* 2007, 2008).

Sample Z-13 was collected from the KKF ductile shear zone in the North Ayilari Range. The zircons record magmatic or metamorphic fluid activity during the period 47 Ma and 32–25 Ma. Further, some of the zircons from sample Z-07, which was collected away from the KKF ductile shear zone in North Ayilari, also recorded magmatic or metamorphic fluid activity during the same periods. The zircon ages of the two samples, regardless of whether they were in the fault zone, have similar Cenozoic magmatic or metamorphic information, indicating that the activity of the KKF had no effect on the growth of the zircon. It is suggested that the THB magmatism that occurred at 45–50 Ma and 32–25 Ma affected some of the zircons in the Animaqing Group. If this is correct, then this implies that deformation associated with movement along the KKF is initially recorded in the THB and Animaqing Group at 12 Ma, as dated by the authigenic mica age in the ductile zone (Valli *et al.* 2007; Wang *et al.* 2011).

Granite of Ordovician age (SK-7 and SK-8) was later deformed in the KKF ductile shear zone in the South Ayilari, but the zircon U–Pb ages of samples SK-7 and SK-8 do not record any Cenozoic magmatic or metamorphic fluid activity, indicating that KKF deformation did not result in the formation of new zircon rims. This is the same scenario as with the 60 Ma and 45–50 Ma THB granites involved in the KKF ductile shear zone in the South Ayilari

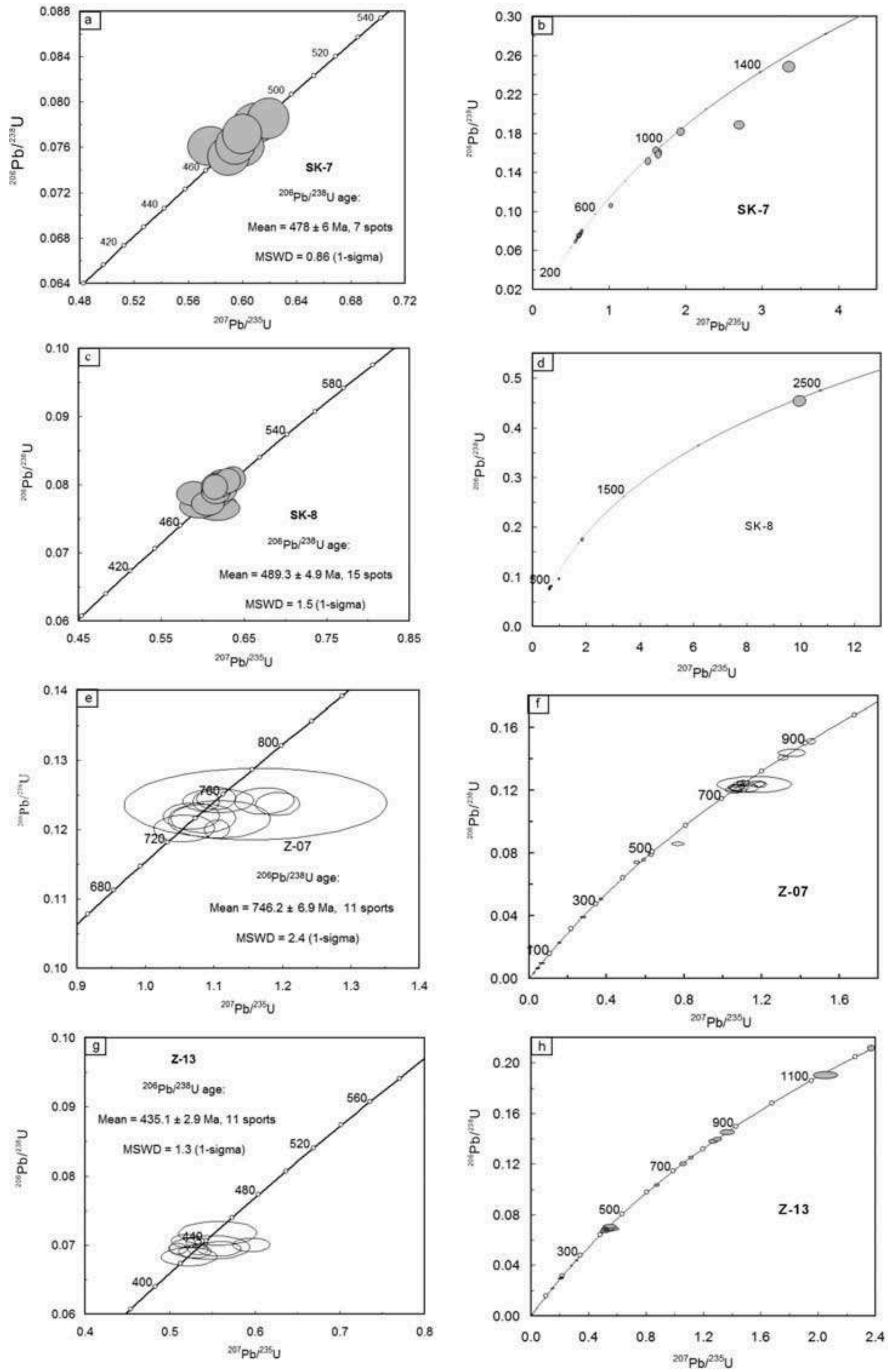

Figure 4. Concordia diagram of zircon CASIMS and LA-ICP-MS U–Pb dating of the Animaqing Group.
Note: MSWD, mean square of weighted deviation.

(Wang *et al.* 2009, 2011). Moreover, the mica $^{40}Ar/^{39}Ar$ ages of the Ordvician granites (SK-7 and SK-8) all fall around 12 Ma, similar to the mica $^{40}Ar/^{39}Ar$ ages of THB granites in the KKF ductile zone around Namru (Wang *et al.* 2009, 2011). Therefore, the combined zircon U–Pb data and $^{40}Ar/^{39}Ar$ mica ages strongly support the concept that deformation related to the KKF first initiated in the southern Ayilari Range at ~12 Ma.

New data reported in this article suggest that the KKF propagated to the southern and northern Ayilari Range

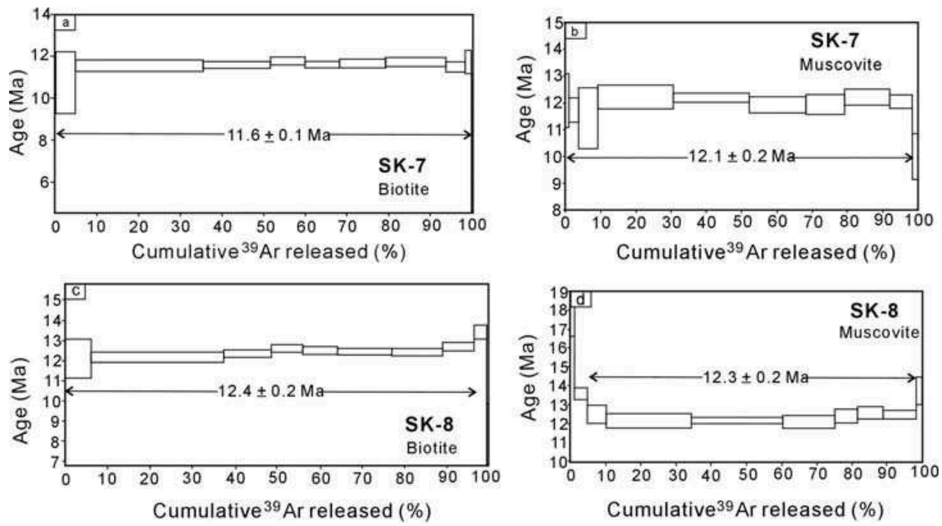

Figure 5. $^{40}Ar/^{39}Ar$ age release spectra for mica.
Note: MSWD, mean square of weighted deviation.

by 12 Ma. The data do not support the proposal that the initiation time of the KKF was around 32–25 Ma, as deduced from the granite zircon U–Pb ages at the North Ayilari (Valli *et al.* 2007). Below, we highlight additional concerns regarding earlier movement along the KKF (in the period 32–25 Ma) as outlined by, for example, Valli *et al.* (2007).

(1) Given that the KKF is dominantly strike slip with an offset of 52–60 km (e.g. Murphy *et al.* 2000; Wang *et al.* 2012) and since age data in the South Ayilari suggest movement at ~12 Ma (Wang *et al.* 2009, 2011, this article), transfer structures should exist between the northern and southern Ayilari Range to absorb such a large offset if the movement of the KKF is around 32–25 Ma at the North Ayilari as Valli *et al.* (2007) suggest. However, the geological features of the Ayilari ranges do not show such features (e.g. Murphy *et al.* 2000; Wang *et al.* 2008a).
(2) Thermo-chronological data from the ductile shear zone in the same area should record similar thermal events associated with fault activity, such as the 12 Ma mica $^{40}Ar/^{39}Ar$ age in the southern and northern Ayilari Range. However, based on the growth of zircons in the ductile zone around the South Ayilari, the cooling history of the rocks in the KKF ductile zone endured none of the thermal events manifested in the North Ayilari granite at 32–25 Ma.
(3) The 32–25 Ma magmatism is widespread in the 2000 km-long THB (e.g. Harrison *et al.* 2000; Chung *et al.* 2003, 2005; Mo *et al.* 2006). Wang *et al.* (2009) also report evidence of a 32 Ma episode of magmatism far away from the ductile shear zone in the South Ayilari. It appears that the 32–25 Ma magmatism resulted from regional magmatic events in the Lhasa block, rather than from syn-kinematic granites related to the KKF.

A model for the role of KKF in Tibetan deformation

Leloup *et al.* (2011) summarized almost all the zircon U–Pb age data along the entire KKF zone, and these data show that granite age dates between 32–25 Ma are derived only from the northern Ayilari Range. These authors also found an 18–16 Ma age for the KKF at the middle segment of the fault, as had Searle *et al.* (1998) and Phillips *et al.* (2004). Since all the data in this article suggest that the North Ayilari granite is not syn-kinematic granite of the KKF, we conclude that the KKF initiated its strike slip after 18 Ma in the middle part of the KKF trace and it propagated southeastward into southwestern Tibet around 12 Ma.

The KKF offsets the GCT fault in the Namru–Menshi basin (Figure 1). This thrust fault was active before 13 Ma, having been offset by the KKF by about 52–66 km (Yin *et al.* 1999; Murphy *et al.* 2000; Wang *et al.* 2012). If the displacements show the greatest offsets along the southern segment of the KKF, one can calculate a long-term slip rate of 4.3 ± 0.2 mm/year based on the 12 Ma initiation time in this segment of the KKF. Our calculated slip rate of ~4.3 mm/year indicates that the fault has undergone a slow average slip since ~12 Ma. Previous studies show that most of the 66–52 km offset has been absorbed by the Zhada–Ayilari–Menshi basin-range system (Wang *et al.* 2008a, 2008b) and the Gurla Mandhata detachment system (Murphy *et al.* 2000, 2002). To the east, the fault trace

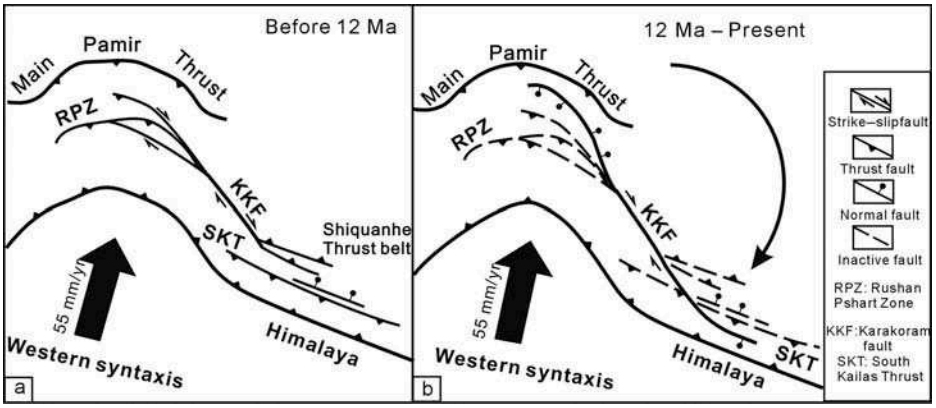

Figure 6. Tectonic model for the spatial and temporal evolution of the KKF (After Robinson 2009; Wang *et al.* 2011). Continuing northward movement of the western syntaxis resulted in the propagation of the KKF into the Gar-Pulan area with a distributed deformation manner.

becomes discontinuous and finally disappears in the middle of southern Tibet (Murphy *et al.* 2010). These observations indicate a distributed deformation character of the fault (Figure 6), rather than large-scale crustal extrusion suggested by Leloup *et al.* (2013); Valli *et al.* (2007, 2008); and Lacassin *et al.* (2004).

Conclusions

New zircon U–Pb ages demonstrate that Ordovician migmatite (489, 478, and 435 Ma) from the footwall of the Ayi Shan detachment was later deformed within the KKF ductile shear zone. Proterozoic gneiss of the Animaqing Group is also part of the detachment footwall. Zircons in the South Ayilari mylonitic migmatites were unaffected by activity along the KKF; similar Cenozoic magmatic and metamorphic data recorded in mylonites and undeformed rocks of the Animaqing Group also rule out the possibility that KKF movement influenced the growth of North Ayilari zircons. The Cenozoic information recorded in the North Ayilari zircons reflects magmatism at 45–50 Ma and 32–25 Ma. Based on zircon U–Pb age and mica $^{40}Ar/^{39}Ar$ ages from mylonites and undeformed rocks, it appears that the KKF first deformed the Animaqing Group and THB granites at ~12 Ma Thus, we interpret the 12 Ma mica age in the ductile shear zone as evidence for the initiation time of the KKF movement in the Ayilari Range. Whilst slip along the central segment of the fault, in Ladakh, northwest India, was initiated at ~16 Ma, our data suggest that the fault lengthened its trace along strike into the Namru–Menshi area at ~12 Ma. Chronologic, kinematic, and geometric studies of the KKF demonstrate that the fault propagated southeastward into SW Tibet in a distributed manner.

Acknowledgements

This research was funded jointly by China Geological Survey (grant No. 1212010914025, 1212011120099) and the National Natural Science Foundation of China (41172192, 40672142). We would like to thank Drs Li, Qiuli, Lai Qingzhou, and Ding Lin for their assistance with $^{40}Ar/^{39}Ar$ and U–Pb data measurement. Thanks also to Betsy Armstrong for her help in revising the draft of the article.

References

Andersen, T., 2002, Correction of common lead in U–Pb analyses that do not report 204Pb: Chemical Geology, v. 192, p. 59–79.

Armijo, R., Tapponnier, P., and Han, T.L., 1989, Late Cenozoic Right-lateral strike-slip faulting in southern Tibet: Journal of Geophysical Research, v. 94, p. 2787–2838.

Bureau of Geology and Mineral Resource of Xizang Province (Xizang BGMR), 1993, In regional geology of Xizang autonomous regions: Beijing, Geological Publishing House, 730 p.

Bureau of Geology and Mineral Resource of Xizang Province (Xizang BGMR), 2005, 1:250000 Regional geology of Shiquanhe: (unpublished).

Chen, Z., Liu, Y., Hodges, K.V., Burchfiel, B.C., Royden, L.H., and Deng, C., 1990, The Kangmar Dome: A metamorphic core complex in southern Xizang (Tibet): Science, v. 250, p. 1552–1556.

Chung, S.L., Chu, M.F., Zhang, Y., Xie, Y., Lo, C.H., Lee, T.Y., Lan, C., Li, X., Zhang, Q., and Wang, Y., 2005, Tibetan tectonic evolution inferred from spatial and temporal variations in post-collisional magmatism: Earth Science Review, v. 68, p. 173–196.

Chung, S.L., Liu, D.Y., Ji, J.Q., Chu, M.F., Lee, H.Y., Wen, D.J., Lo, C.H., Lee, T.Y., Qian, Q., and Zhang, Q., 2003, Adakites from continental collision zones: Melting of thickened lower crust beneath southern Tibet: Geology, v. 31, p. 1021–1024.

Harrison, T.M., Yin, A., Grove, M., Lovera, O.M., Ryerson, F.J., and Zhou, X., 2000, The Zedong Window: A record of superposed Tertiary convergence in southeastern Tibet: Journal of Geophysical Research, v. 105, p. 19211–19230.

Ji, W.H., Chen, S.J., Zhao, Z.M., Li, R.S., He, S.P., and Wang, C., 2009, Discovery of the Cambrian1667 volcanic rocks in the Xainza area, Gangdese orogenic belt, Tibet, China and its significance: Geological Bulletin of China, v. 9, p. 1350–1354. [In Chinese with English abstract.]

Lacassin, R., Valli, F., Arnaud, N., Leloup, P.H., Paquette, J.L., Li, H., Tapponnier, P., Chevalier, M.L., Guillot, S., Maheo, G., and Xu, Z., 2004, Large-scale geometry, offset and kinematic evolution of the Karakorum fault, Tibet: Earth and Planetary Science Letters, v. 219, no. 3–4, p. 255–269.

Lee, J., Dinklage, W.S., Hacker, B.R., Wang, Y., Gans, P.B., Calvert, A., Wan, J., Chen, W., Blythe, A., and McClelland, W., 2000, Evolution of the Kangmar Dome, southern Tibet: Structural, petrologic, and thermochronologic constraints: Tectonics, v. 19, p. 872–896.

Leloup, H.P., Weinberg, F.R., Mukherjee, K.B., Tapponnier, P., Lacassin, R., Boutonnet, E., Chevalier, M.-L., Valli, F., Li, H., Arnaud, N., and Paquette, J.-L., 2013, Comment on 'Displacement along the Karakoram fault, NW Himalaya, estimated from LA-ICP-MS U–Pb dating of offset geologic markers' published by Shifeng Wang *et al*. in EPSL, 2012: Earth and Planetary Science Letters, v. 363, p. 260–263.

Leloup, P.H., Boutonnet, E., Davis, W.J., and Hattori, K., 2011, Long-lasting intracontinental strike-slip faulting: New evidence from the Karakorum shear zone in the Himalayas: Terra Nova, v. 23, no. 2, p. 92–99.

Li, X., Liu, Y., Li, Q., Guo, C., and Chamberlain, K., 2009, Precise determination of Phanerozoic zircon Pb/Pb age by multicollector SIMS without external standardization: Geochemistry, Geophysics, Geosystems, v. 10, no. 4, p. Q04010, doi:10.1029/2009GC002400.

Liu, Q., 1993, Pale.oclimats et contraintes chronologiques surles mouvements re.cents dans l'ouest du Tibet: failles du Karakorum et de Longmu CôGozha Co, lacs en pulla-part de Longmu Co et de Sumxi Co. [PhD]: Universite. Paris 7.

Ludwig, K.R., 2001, Users manual for Isoplot/Ex rev. 2.49, Spec. Publ. 1a, Berkeley Geochronol. Cent., Berkeley, Calif.

Miller, C., Schuster, R., Klotzli, U., Frank, W., and Grasemann, B., 2000, Late Cretaceous–Tertiary magmatic and tectonic events in the Transhimalaya batholith (Kailas area, SW Tibet): Schweizerische Mineralogische und Petrographische Mitteilungen, v. 80, p. 1–20.

Mo, X., Zhao, Z., Deng, J., Flower, M., Yu, X., Luo, Z., Li, Y., Zhou, S., Dong, G., Zhu, D., and Wang, L., 2006, Petrology and geochemistry of postcollisional volcanic rocks from the Tibetan plateau: Implications for lithosphere heterogeneity and collision-induced asthenospheric mantle flow: Geological Society of America Special Paper, v. 409, p. 507–530.

Murphy, M.A., Sanchez, V., and Taylor, M.H., 2010, Syncollisional extension along the India–Asia suture zone, south-central Tibet: Implications for crustal deformation of Tibet: Earth and Planetary Science Letters, v. 290, p. 233–243.

Murphy, M.A., Yin, A., Kapp, P., Harrison, T.M., Din, L., and Guo, J., 2000, Southward propagation of the Karakorum fault system into southwest Tibet: Timing and magnitude of slip: Geology, v. 28, p. 451–454.

Murphy, M.A., Yin, A., Kapp, P., Harrison, T.M., Manning, C.E., Ryerson, F.J., Din, L., and Guo, J., 2002, Structural evolution of the Gurla Mandhata detachment system, southwest Tibet: Implications for the eastward extent of the Karakorum fault system: Geological Society of America Bulletin, v. 114, p. 428–447.

Peltzer, G., and Tapponnier, P., 1988, Formation and evolution of strike-slip faults, rifts, and basins during the India–Asia collision: An experimental approach: Journal of Geophysical Research, v. 93, p. 15085–15117.

Phillips, R.J., Parrish, R.R., and Searle, M.P., 2004, Age constraints on ductile deformation and long-term slip rates along the Karakorum fault zone, Ladakh: Earth and Planetary Science Letters, v. 226, p. 305–319.

Phillips, R.J., and Searle, M.P., 2007, Macrostructural and microstructural architecture of the Karakoram fault: Relationship between magmatism and strike-slip faulting: Tectonics, v. 26, p. TC3017, doi:10.1029/2006TC001946.

Phillips, R.J., Searle, M.P., and Parrish, R.R., 2013, The geochemical and temporal evolution of the continental lithosphere and its relationship to continental-scale faulting: The Karakoram Fault, Eastern Karakoram, NW Himalaya: Geochemistry Geophysics Geosystems, v. 14, p. 583–603, doi:10.1002/ggge.20061.

Quigley, M., Yu, L., Liu, X., Wilson, C., Sandiford, M., and Phillips, D., 2006, 40Ar/39Ar thermochronology of the Kampa Dome, southern Tibet: Implications for tectonic evolution of the North Himalayan gneiss domes: Tectonophysics, v. 421, p. 269–297.

Ratschbacher, L., Frisch, W., and Liu, G., 1994, Distributed deformation in southern and western Tibet during and after the India-Asia collision: Journal of Geophysical Research, v. 99, p. 19917–19945.

Robinson, A., Ducea, M., and Lapen, T., 2012, Detrital zircon and isotopic constraints on the crustal architecture and tectonic evolution of the northeastern Pamir: Tectonics, v. 31, doi:10.1029/2011TC003013.

Robinson, A.C., 2009, Geologic offsets across the northern Karakorum fault: Implications for its role and terrace correlations in the western Himalayan-Tibetan orogen: Earth and Planetary Science Letters, v. 279, p. 123–130.

Robinson, A.C., Yin, A., Manning, C.E., Harrison, T.M., Zhang, S.-H., and Wang, X.-F., 2004, Tectonic evolution of the northeastern Pamir: Constraints from the northern portion of the Cenozoic Kongur Shan extensional system, western China: Geological Society of America Bulletin, v. 116, p. 953–973.

Sanchez, V., Murphy, A.M., Dupré, R.W., Ding, L., and Zhang, R., 2010, Structural evolution of the Neogene Gar Basin, western Tibet: Implications for releasing bend development and drainage patterns: Geology Society of American Bulletin, v. 122, no. 5–6, p. 926–945.

Saylor, J.E., Quade, J., Dettman, D.L., DeCelles, P.G., Kapp, P.A., and Ding, L., 2009, The late Miocene through present paleoelevation history of southwestern Tibet: American Journal of Science, v. 309, p. 1–42.

Searle, M.P., 1996, Geological evidence against large-scale pre-Holocene offsets along Karakorum fault: Implications for the limited extrusion of the Tibetan plateau: Tectonics, v.15, p. 171–186.

Searle, M.P., Elliott, J.R., Phillips, R.J., and Chung, S.L., 2011, Crustal-lithospheric structure and continental extrusion of Tibet: Journal of the Geological Society of London, v. 168, p. 633–672, doi:10.1144/0016-76492010-139.

Searle, M.P., and Phillips, R.J., 2004, A comment on Large-scale geometry, offset, and kinematic evolution of the Karakoram fault, Tibet. Q by R. Lacassin *et al*. (Earth Planet. Sci. Lett. 219 (2004) 255–269): Earth and Planetary Science Letters, v. 229, p. 155–158.

Searle, M.P., Weinberg, R.F., and Dunlap, W.J., 1998, Transpressional tectonics along the Karakorum fault zone, northern Ladakh: Constrains on Tibet extrusion, *in* Holdsworth, R.E., ed., Continental transpressional and transtensional tectonics, Geological Society [London] Special Publication, v. 135, p. 307–326.

Sláma, J., Košler, J., Condon, D., Crowley, J., Gerdes, A., Hanchar, J., Horstwood, M., Morris, G., Nasdala, L., Norberg, N., Schaltegger, U., Schoene, B., Tubrett, M., and

Whitehouse, M., 2008, Plesovice zircon: A new natural reference material for U-Pb and Hf isotopic microanalysis: Chemical Geology, v. 249, p. 1–35.
Steiger, R.H., and Jager, E., 1977, Subcommission on geochronology: Convention on the use of decay constraints in geo- and cosmo-chronology: Earth and Planetary Science Letters, v. 36, p. 359–362.
Valli, F., Arnaud, N., Leloup, H.P., Sobel, E.R., Maheo, G., Lacassin, R., Guillot, S., Li, H., Tapponnier, P., and Xu, Z., 2007, Twenty million years of continuous deformation along the Karakorum fault, western Tibet: A thermochronological analysis: Tectonics, v. 26, doi 10.1029/2005TC001913.
Valli, F., Leloup, P., Paquette, J., Arnaud, N., Li, H., Tapponnier, P., Lacassin, R., Guillot, S., Liu, D., Deloule, E., Xu, Z., and Mahéo, G., 2008, New U-Th/Pb constraints on timing of shearing and long-term slip-rate on the Karakorum fault: Tectonics, v. 27, doi 10.1029/2007TC002184.
Wang, S., Blisniuk, P., Kempf, O., Fang, X., Fan, C., and Wang, E., 2008a, The Basin – Range System along the South Segment of the Karakorum Fault Zone, Tibet: International Geology Review, v. 50, p. 121–134.
Wang, S., Fang, X., Lai, Q., Zheng, D., and Wang, Y., 2009, New radiometric dating constrains the time for initiation of the Karakorum fault zone (KFZ), SW Tibet: Tectonophysics, v. 475, p. 503–513.
Wang, S., Murphy, M.A., Phillips, R.J., and Wang, C., 2013, Reply to comment on 'Displacement along the Karakoram fault, NW Himalaya, estimated from LA-ICPMS U-Pb dating of offset geologic markers' by Leloup et al. in EPSL, 2012: Earth and Planetary Science Letters, v. 363, p. 246–248.
Wang, S., Wang, C., Phillips, R.J., Murphy, M.A., Xiaomin, F., and Yahui, Y., 2012, Displacement along the Karakoram Fault, NW Himalaya, estimated from LA-ICP-MS U-Pb dating of offset geologic markers: Earth and Planetary Science Letters, v. 337–338, p. 156–163.
Wang, S., Wang, E., Fang, X., and Lai, Q., 2011, U-Pb SHRIMP and 40Ar/39Ar ages constrain the deformation history of the Karakoram fault zone (KFZ), SW Tibet: Tectonophysics, v. 509, p. 208–217.
Wang, S., Zhang, W., Fang, X., Dai, S., and Kempf, O., 2008b, Magnetostratigraphy of the Zanda basin in southwest Tibet Plateau and its tectonic implications: Chinese Science Bulletin, v. 53, no. 9, p. 1393–1400.
Yin, A., Harrison, T.M., Murphy, M.A., Grove, M., Nie, S., Ryerson, F.J., Wang, X., and Chen, Z., 1999, Tertiary deformation history of southeastern and southwestern Tibet during the Indo-Asian collision: Geological Society of America Bulletin, v. 111, p. 1644–1664.
Zhang, R., Murphy, M.A., Lapen, T.J., Sanchez, V., and Heizler, M., 2011, Late Eocene crustal thickening followed by Early-Late Oligocene extension along the India-Asia suture zone: Evidence for cyclicity in the Himalayan orogen: Geosphere, v. 7, p. 1249–1268.
Zhu, D., Zhao, Z., Niu, Y., Dilek, Y., Hou, Z., and Mo, X., 2012, Origin and pre-Cenozoic evolution of the Tibetan Plateau: Gondwana Research, doi: 10.1016/j.gr.2012.02.002.